Interface Engineering of Mesoporous Triphasic Cobalt-Copper Phosphides as Active Electrocatalysts for Overall Water Splitting

Ali Saad,[a] Zhixing Cheng,[a,b] Hangjia Shen,[a,b]Haichuan Guo, [a,b] John Paul Attfield,[c]*Tiju Thomas, [d]* Minghui Yang [a,b]*

[a] Ningbo Institute of Materials Technology and Engineering Chinese Academy of Sciences Ningbo 315201, China. E-mail: myang@nimte.ac.cn

[b] Center of Materials Science and Optoelectronics Engineering, University of Chinese Academy of Sciences, Beijing 100049, China.

[c] Centre for Science at Extreme Conditions and School of Chemistry University of Edinburgh Kings Buildings, West Mains Road, Edinburgh EH9 3JJ, UK E-mail: j.p.attfield@ed.ac.uk

[d] Department of Metallurgical and Materials Engineering Microstructure Indian Institute of Technology Madras Adyar Chennai 600036, Tamil Nadu, India. E-mail: tt332@cornell.edu, tijuthomas@iitm.ac.in

Table of Contents

1Experimental Section

1-1 Material:

Pluronic P123 triblock copolymer ($EO_{20}PO_{70}EO_{20}$) [Mw = 5800], tetraethylorthosilicate (TEOS, 98%), n-Butanol, concentrated HCl (37% wt%, AR) are purchased from Aladdin Industrial Corporation (Shanghai, China), sodium hydroxide (NaOH 90%), Copper(II) nitrate trihydrate ($Cu(NO_3)_2$ $3H_2O$), Cobalt nitrate hexahydrate ($Co(NO_3)_2 \cdot 6H_2O$), Sodium hypophosphite ($NaPO_2H_2$, 99%), potassium hydroxide (KOH, 99%) and IrO_2/C (20% Iron Vulcan XC-72).Highly dispersed platinum 20wt% in carbon is represented as commercial Pt/C in this study. Nafion solution (5 wt %) is purchased from Du Pont Corp. All chemicals are used as received without any further purification deionized water and ethanol is used throughout the experiment.

1-2 Materials synthesis:

1-2-1 Synthesis of KIT-6 mesoporous silica:

The mesoporous KIT-6 is synthesized in acidic conditions following the procedure according to Kleitz et al.[1]First, 6g of nonionic triblock copolymer Pluronic P123 is dissolved in a mixture of 220 ml of water and 12g of HCl (37%). Thus, the solution is vigorously stirred for 6 h at 35 °C. After complete dissolution of Pluronic P123, 6 g of butanol is added while ensuring continuous stirring for another hour. Next, 12.48 g of TEOS is added at once to the solution. Stirring is continued for 24 hours. The mixture is left under stirring at 35 °C for 24 h, followed by a hydrothermal treatment at 50 °C under static conditions for 24 h. The resultant white product is filtered without washing and dried for 24 h at 90°C. Finally, the products are calcined in flowing air at 550°C for 6 h at a heating rate of 2°C min^{-1}.

1-2-2 Synthesis of ordered mesoporous oxides (Co_3O_4, CuO, Co_2CuO4, $CoCuO_x$ and Cu_2CoO_x):

Crystalline mesoporous oxides are prepared using a hard-templating method using mesoporous KIT-6 according to Kleitz et al. 0.8 M of metal nitrates as a precursor ($Co(NO_3)_2 \cdot 6H_2O$), ($Cu(NO_3)_3$ $9H_2O$) are dispersed in 3.6 mL of ethanol in a molar ratio of (1:0 0:1, 2:1, 1:1 and 1:2) for Co_3O_4, CuO, Co_2CuO4, $CoCuO_x$ and Cu_2CoO_x, respectively. To this solution, 0.5 g KIT-6 is dispersed and heated at 60 °C under vigorous stirring until ethanol is evaporated. Then the resulting precursors/silica composite is heated in a ceramic crucible in an oven at 250 °C for

4 h. In order to achieve higher loadings, the impregnation step is repeated to ensure the complete filling of the pores of KIT-6 with metal oxides. Again, after evaporation of the solvent, the resulting metal precursor/silica composites are calcined at 550 °C for 6 h. The silica template is removed using treatment with 2 M NaOH solution, followed by washing with deionized water and ethanol. This in turn is followed up with vacuumdrying at 60°C.

1-2-3 Synthesis of ordered mesoporous phosphides:

In order to prepare the corresponding phosphides from the above mesoporous oxides, 50 mg of ordered mesoporous oxides and 1g of $NaH_2PO_2 \cdot H_2O$ are put at two separate positions of a porcelain in a ceramic boat inside at the upstream of the gas flow (Figure S3 shows optical photographs of an example of samples before and after phosphorization). The weight ratio of mesoporous oxides-to-phosphorus (P) is set to 1:20. Subsequently, after purging with N_2, the center of the furnace is elevated to 390°C, 300°C and 360°C for CoP, Cu_3P and bimetallic Co-Cu phosphides, respectively for 3 h at a ramping rate of 4 °C min^{-1}. Finally the furnace was naturally cooled to room temperature.

1-3 Structural and surface characterization:

XRD measurements are conducted using X-ray diffraction (XRD) from a Miniflex600 X-ray diffractometer using monochromatic Cu K_α radiation at a scanning rate of 1°/min (λ = 0.1542 nm, accelerating voltage 40 kV, and applied current 15). Low-angle X-ray diffraction (XRD) data are recorded on Bruker AXS diffractometer System from 0.5 to 5 (2θ). Textural and morphology of the samples examined using a JEM-2100 instrument (Japan) andfield-emission scanning electron microscope (FE-SEM, Hitachi S4800, Japan) mounted with energy dispersive X-ray spectroscopy (EDS), respectively. Chemical compositions of the samples are determined by using an AXIS ULTRA DLD (Shimadzu, Japan) x-ray photoelectron spectroscopy (XPS) with a non-monochromatized Al-K_α X-ray19 as the excitation source. Binding energy calibration is based on C 1s at 284.8 eV. Surface area measurements are performed by nitrogen adsorption using Brunauere Emmet Teller (BET) area method whereas mesopore size is assessed by the Barrett−Joyner−Halenda (BJH) method from the desorption branch of the isotherm.

1-4 Electrochemical measurements:

The electrochemical measurements are conducted in a three compartment electrochemical cell equipped an Ag/AgCl saturated electrode (in a saturated KCl solution) as the reference electrode and counter electrode is platinum Pt sheet (1 cm× 1cm). A glassy carbon electrode (GCE) with a diameter of 5 mm (0.196 cm^2 surface areas) is used as the working electrode.

The electrode material is prepared by dispersing 4 mg of the catalyst and 25 μL of Nafion solution (DuPont, 5 wt%) are dispersed in a 1mL of mixed solution 750 μL of ethanol and 250 μL of water. The mixture is then sonicated for at least 40 min to form a homogeneous ink. 10 μL of the resulting dispersion were deposited on the glassy carbon electrode with a fixed mass loading (0.203 mg cm^{-2}). The same procedure is used for all of the samples during their electrode preparation. Before the OER and HER measurement are carried out, the electrolyte (1 M KOH) is saturated with O_2 and N_2, respectively for at least 30 min. In order to activate the electrocatalysts, the cyclic voltammetry (CV) measurement are performed at 5 mV s^{-1} from 1.2 -1.8 V (vs RHE) at 1600 rpm for OER. While for the HER measurements, the CV measurement is performed in the range of 0−0.7 to 0 V versus RHE.

The conversion between potentials vs Ag/AgCl and vs RHE is performed using the following equation:
$E_{RHE} = E_{Ag/AgCl} + 0.0591\, pH + 0.197$

The overpotential (η) is calculated according to the following formula:

$$\eta(V) = E_{RHE} - 1.230$$

The ECSA is evaluated based on the double-layer capacitance (C_{dl}) of the electrodes – electrolyte interface using cyclic voltammetry in a small potential range (01.04–1.12V vs RHE), from which the double layer capacitance is determined from the slope of capacitive current (1.1 V vs RHE) versus the scan rate according to[2]:

$$C_{dl} = \frac{\Delta Q}{\Delta V} = \frac{j}{v}$$

The ECSA can be calculated from the C_{dl} according to the ratio:

$$ESCA = \frac{C_{dl}}{C_S}$$

Where Cs is the specific capacitance, chosen as Cs = 0.040 mF·cm^{-2} in 1 M KOH based on reported values.[3] To test the long term performance of the electrocatalysts, the chronopotentiometric (CP) curve is conducted out at a fixed current density using carbon graphite as the counter electrode The long time durability test s conducted by using controlled-potential electrolysis method without iR compensation.The ECSA can be calculated from the C_{dl} according to the ratio:
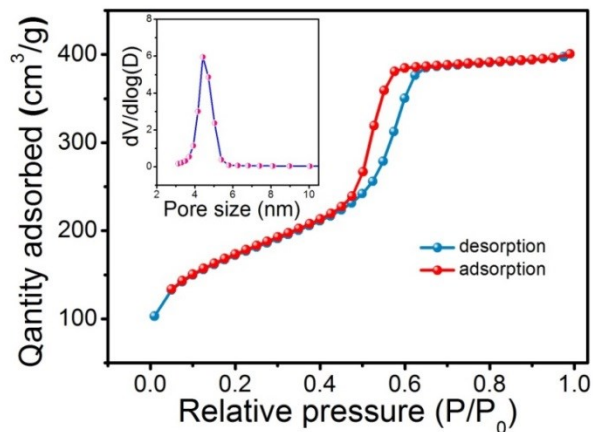
$$ESCA = \frac{C_{dl}}{C_S}$$

Where C_s is the specific capacitance, chosen as C_s = 0.040 mF·cm^{-2} in 1 M KOH based on reported values.

1-2 Supporting Figures:
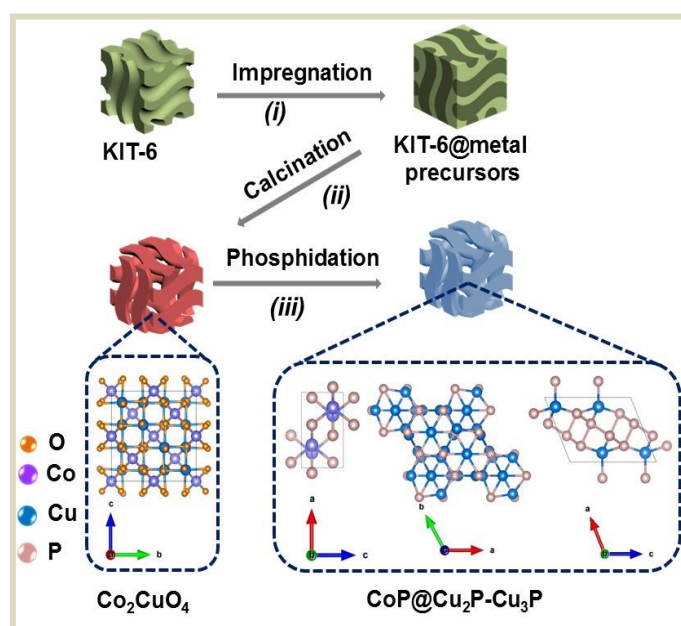
FigureS1. Schematic illustration of the synthetic strategy for ordered mesoporous triphasic CoP@Cu$_2$P-Cu$_3$P phosphides.

Figure S2. Nitrogen adsorption/desorption isotherms of KIT-6 (the inset shows the BJH pore-size distribution). The BET specific surface area of the as-synthesized KIT-6 template is 613.48 m^2g^{-1} with a pore volume of 0.61 cm^3g^{-1} and pore diameter of 5.037 nm.
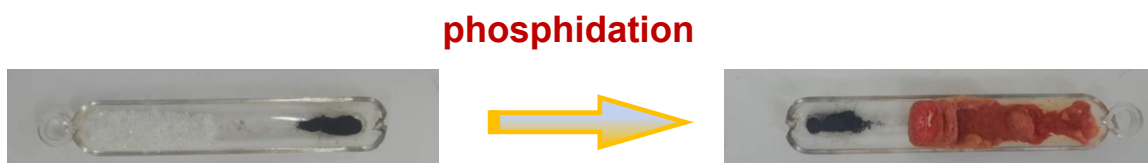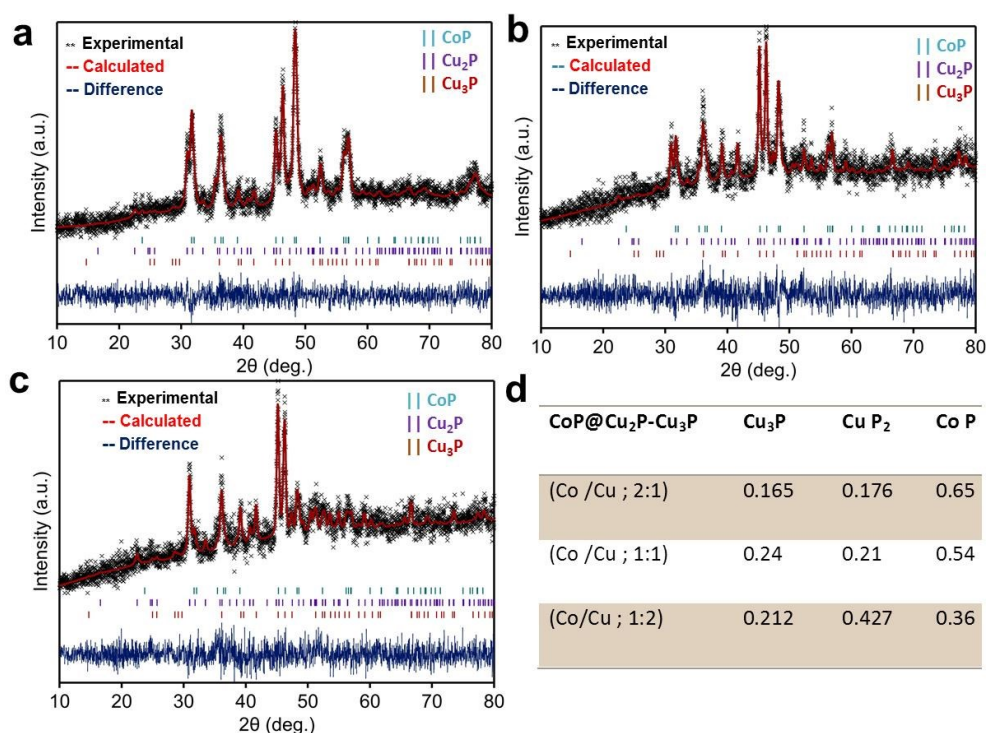
phosphidation

Figure S3. Optical photographs of an example of as prepared mesoporous phosphides catalysts before and after phosphorization.
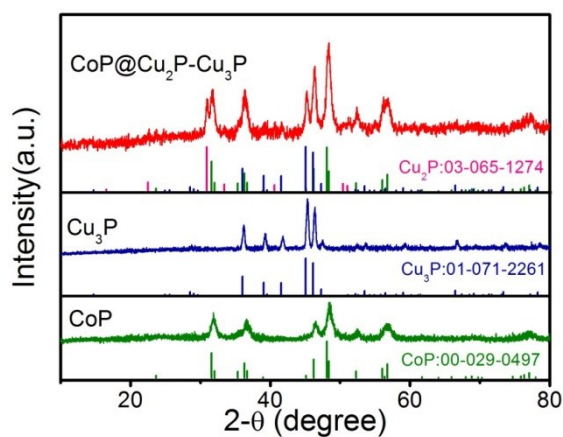
**Figure S4.** Wide-angle XRD patterns of mesoporous CoP, Cu_3P and triphasic $CoP@Cu_2P-Cu_3P$ phosphides.
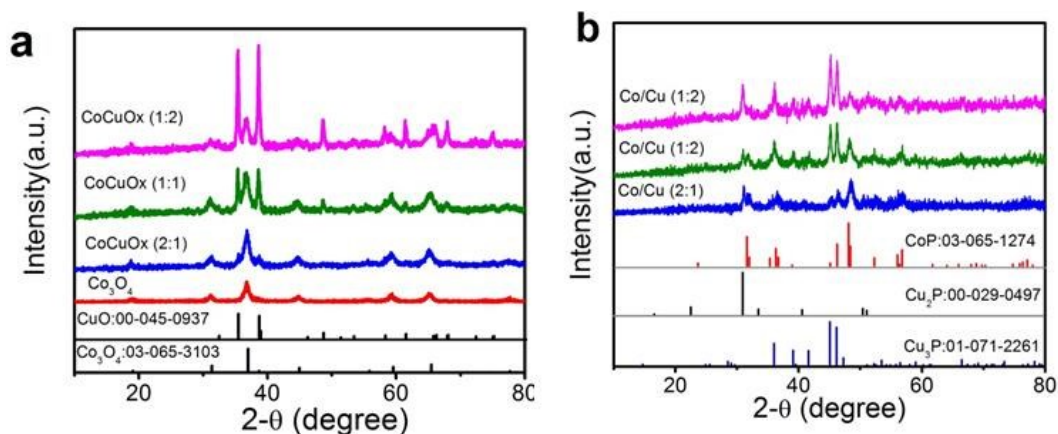
FigureS5. Wide-angle XRD pattern of (a) mesoporous Co-Cu oxides phosphides with different Co: Cu ratio, (b) their corresponding mesoporous phosphides. XRD patterns as shown in Figure S3a display well-defined diffraction peaks could all be indexed to Co_3O_4 (JCPDS Card No. 03-065-3103) and CuO (JCPDS Card No. 00-045-0937). After phosphorization, the patterns of mesoporous triphasic phosphides show mixed phases indexed to CoP phase (JCPDS card 03-065-1274), Cu_2P phase (JCPDS card 00-029-0497) and Cu_3P phase (JCPDS card 01-071-1261).

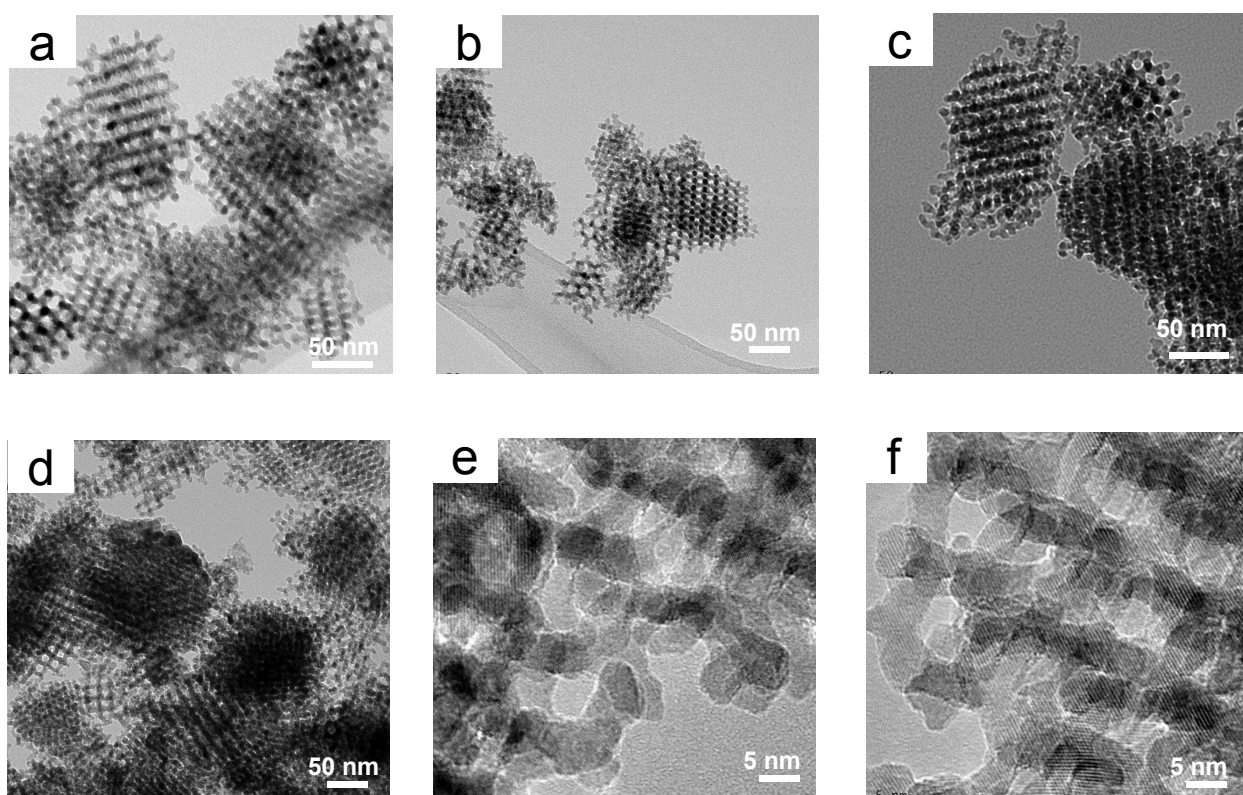| CoP@Cu$_2$P-Cu$_3$P	Cu$_3$P	Cu P$_2$	Co P
(Co /Cu ; 2:1)	0.165	0.176	0.65
(Co /Cu ; 1:1)	0.24	0.21	0.54
(Co/Cu ; 1:2)	0.212	0.427	0.36

Figure S6. Rietveld refined XRD patterns of CoP@Cu$_2$P-Cu$_3$P with theoretical Co/Cu ratio (a) 2:1, (b) 1:1 and (c) 1:2. (d) The mass fraction of metallic phosphides from the Rietveld refined XRD well matching with the expected theoretical values. The Rietveld refinement of the observed XRD patterns confirms the resultant crystalline phases without any detectable impurity (Figure S4a, 4b and 4c). The actual ratio of each phase is determined and the results are listed in Figure S4d.
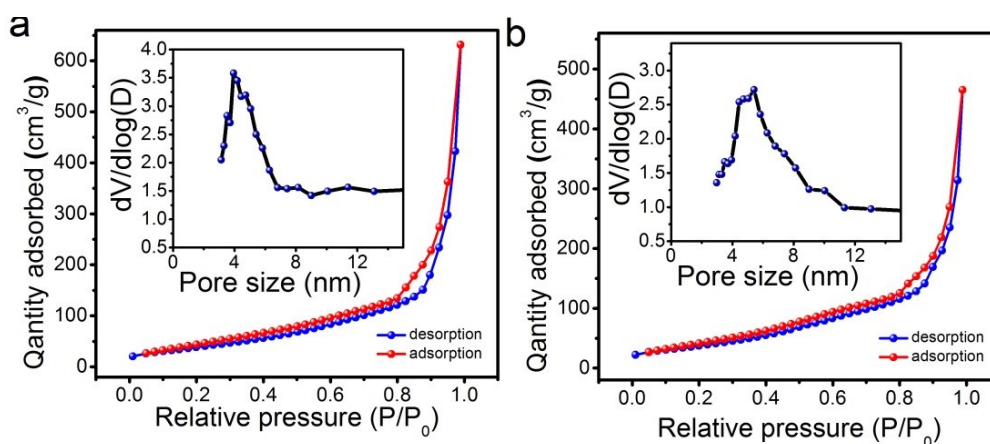
Figure S7. Nitrogen adsorption/desorption isotherms at 77 K (inset pore size distribution calculated with the adsorption branch) for Co_2CuO_4 (a) and $CoP@Cu_2P$-Cu_3P (b). Both samples show type IV isotherms with hysteresis loops as is typical for mesoporous materials. The template-free mesostructured materials have BET surface area of 155.2 and 146.05 m^2g^{-1} with pore size distributions ranging from 4 to 6 nm, for Co_2CuO_4 and $CoP@Cu_2P$-Cu_3P, respectively.


Figure S8. Large-scale TEM images of mesoporous (a) Co_2CuO_4, (b) CoP, (c) Cu_3P and (d)**.** $CoP@Cu_3P$-Cu_2P. Uniform and well-ordered mesopores arranged in three dimensional structures are observed. HRTEM of mesoporous (e) Co_2CuO_4 and (f) triphasic phosphides $CoP@Cu_2P$-Cu_3P.
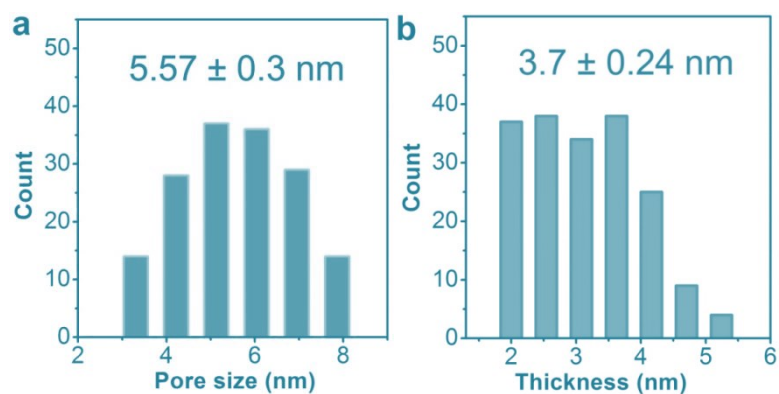
Figure S9. Pore size distribution (a) and the thickness (b) for mesoporous triphasic CoP@Cu$_3$P-Cu$_2$P junction. The diameter of pores and thickness of mesoporous CoP@Cu$_3$P-Cu$_2$P are approximately ~5 .6 nm and ~3.7 nm (Figure S6), respectively.
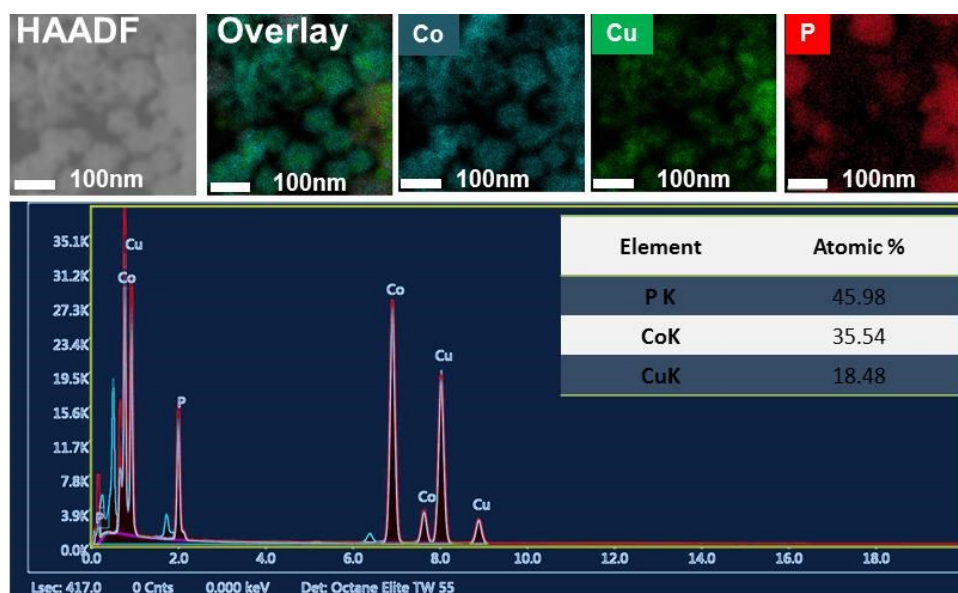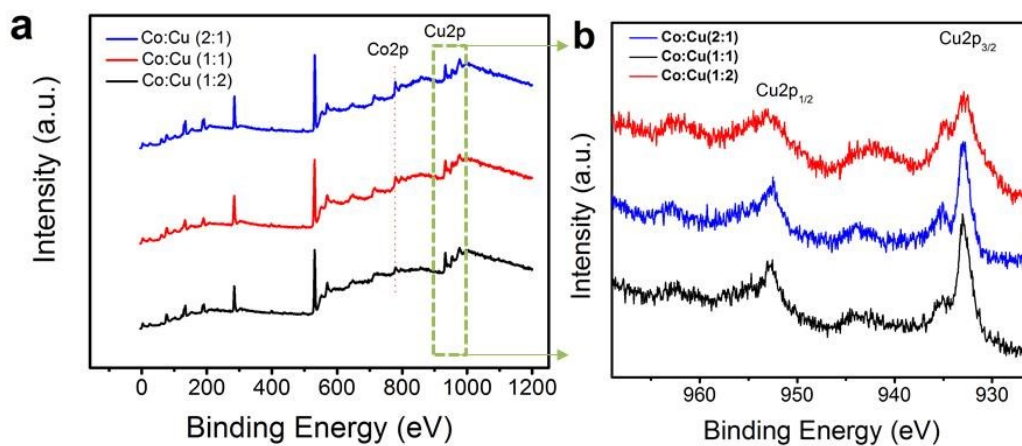

Figure S10. Elemental mapping images of Co, Cu, and P on CoP@Cu$_3$P-Cu$_2$P and EDX spectrum (the atomic ratio of Co/Cu in CoP@Cu$_3$P-Cu$_2$P is estimated around 1.92).
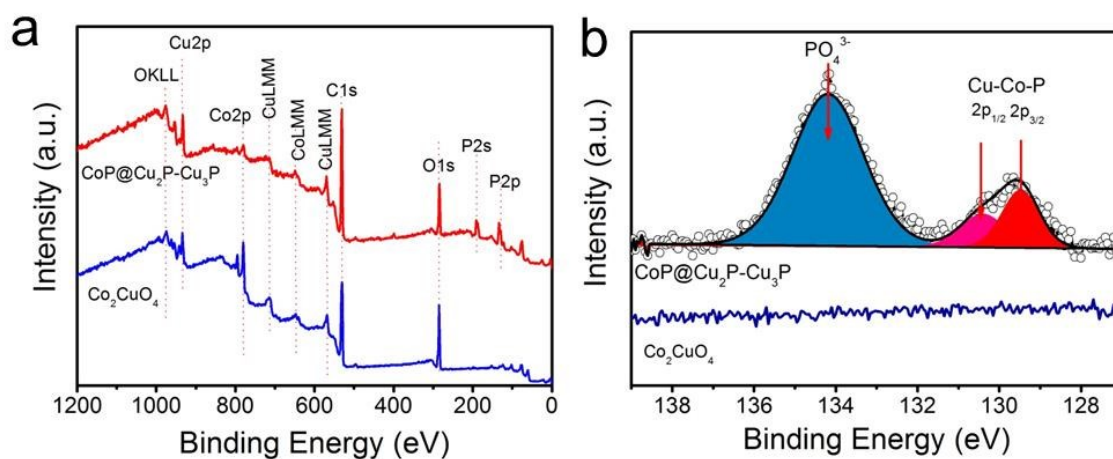
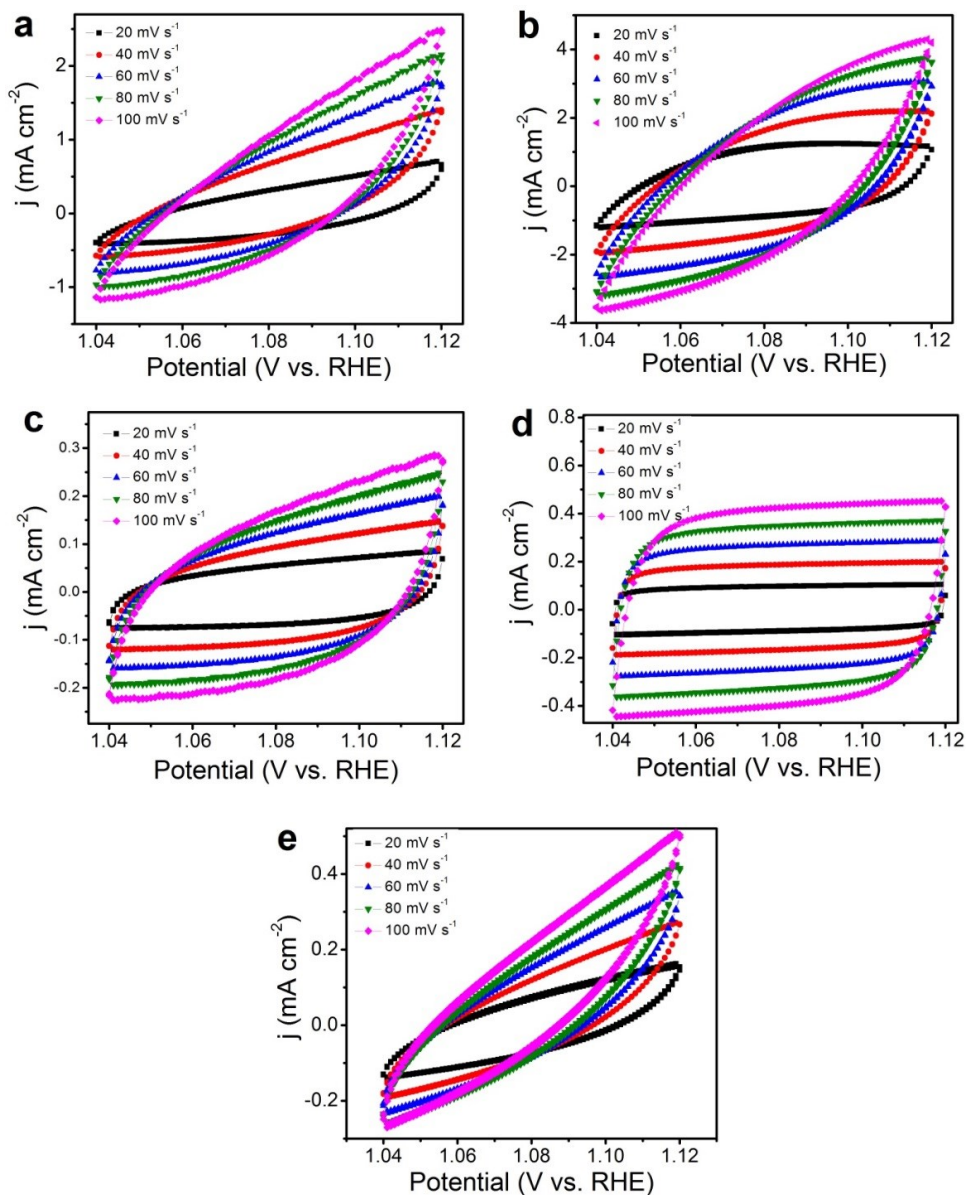**FigureS11.** (a) XPS survey spectrum for Co$_2$CuO$_4$ and CoP@Cu$_2$P-Cu$_3$P. (b) High-resolution XPS spectra P2p for Co$_2$CuO$_4$ and CoP@Cu$_2$P-Cu$_3$P.

Figure S12. (a) XPS survey spectrum for bimetallic Co-Cu phosphides witch different ratio, (b) high resolution Cu regions. The intensity of Cu2p increases by increasing the amount of copper in the triphasic $CoP@Cu_3P-Cu_2P$ system.

Figure S13. Cyclic voltammograms with a scan rate of 20, 40, 60, 80, and 100 mV s^{-1} in 1 M KOH for (a) CoP@Cu$_2$P-Cu$_3$P, (b) CoP, (c) Cu$_3$P, (d) Co$_2$CuO$_4$, and (e) IrO$_2$/C. The mesoporous CoP@Cu$_2$P-Cu$_3$P catalyst provides high cathodic (*i*c) and anodic (*i*a) current densities (cyclic voltammetry (CV) areas) at each scan rate, consistent with a much greater active surface area.
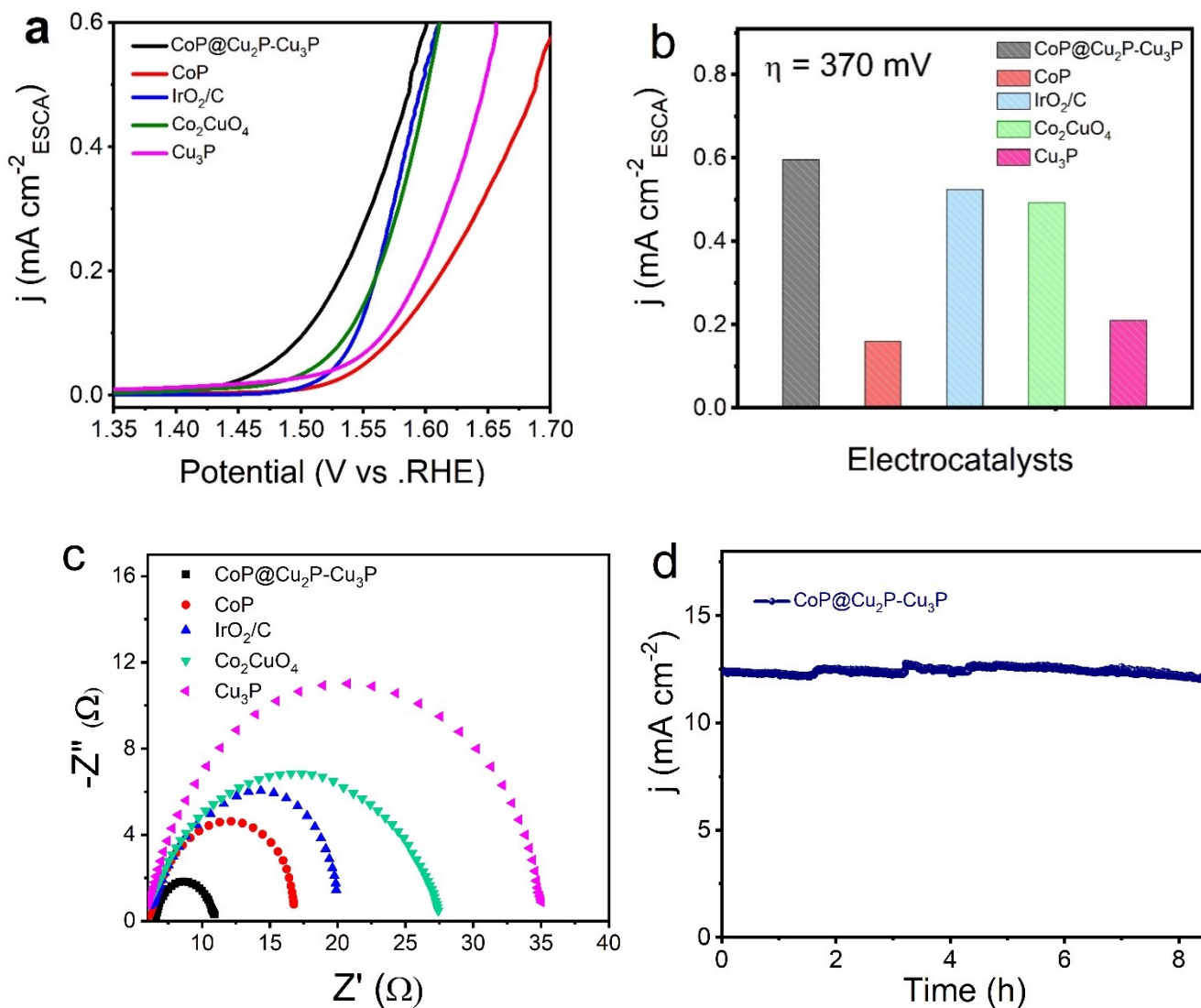
Figure S14. (a) The electrochemically active surface area (ECSA) for linear-sweep voltammetry (LSV) curves and (b) the intrinsic catalyst activity of CoP@Cu$_2$P-Cu$_3$P, CoP, Cu$_3$P, Co$_2$CuO$_4$, and IrO$_2$/C. These results exhibit excellent intrinsic activity and indicating more active sites generated in the associated mesoporous triphasic CoP@Cu$_2$P-Cu$_3$P toward OER activity. (c) Nyquist plots obtained at 270 mV overpotential on mesoporous Co$_2$CuO$_4$, CoP, Cu$_3$P, CoP@Cu$_2$P-Cu$_3$P and benchmark catalyst IrO$_2$/ (d) OER Chronopotentiometric curves for CoP@Cu$_2$P-Cu$_3$P at 1.5 V vs RHE in M KOH solution.

11
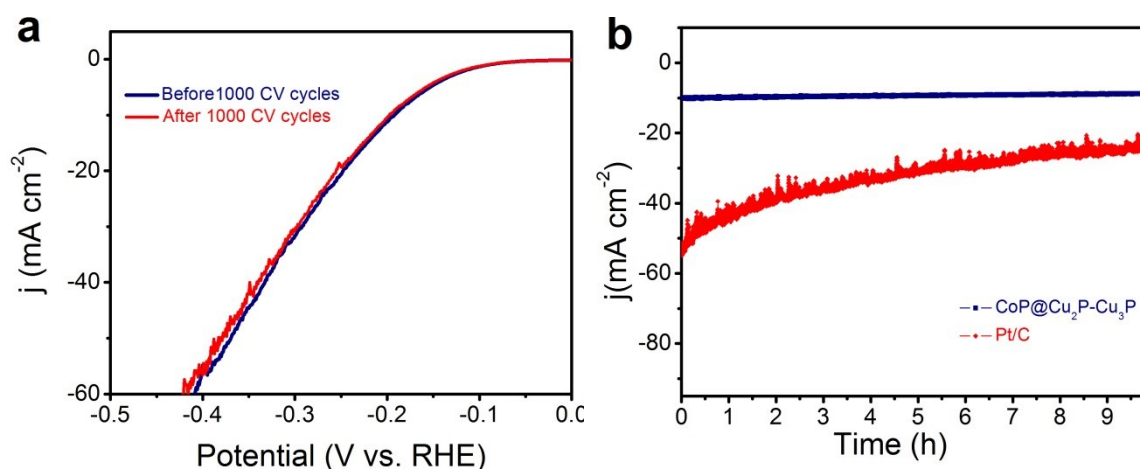
FigureS15. (a) HER polarization curves for CoP@Cu$_2$P-Cu$_3$P before and after 1000 CV cycles. **(b)** Chronopotentiometric curves for CoP@Cu$_2$P-Cu$_3$P at | j |= 10 mA cm^{-2} in 1 M KOH solution.

**Figure S16.** Optical photographs of electrocatalytic water splitting process, showing (a) the three electrode glass cell and bubbles on the surface of working electrode.
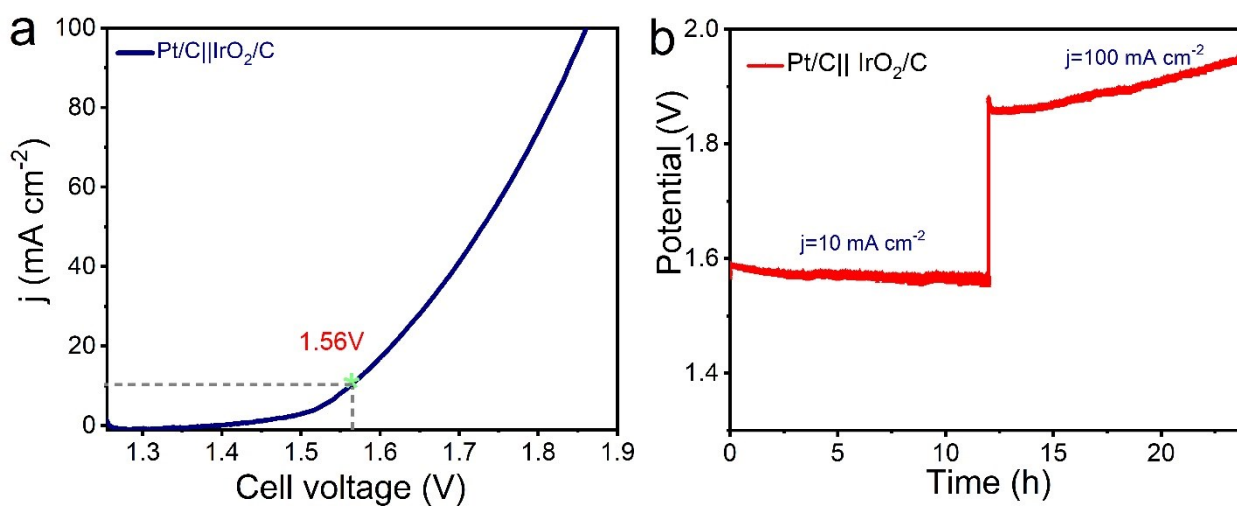
Figure S17.(a) LSV polarization curve without iR compensation for Pt/C‖ IrO$_2$/C electrodes in 1 M KOH for overall water splitting. (c) Durability of overall water splitting for a current density trace of 10−100 cm^{-2} for Pt/C‖ IrO$_2$/C.
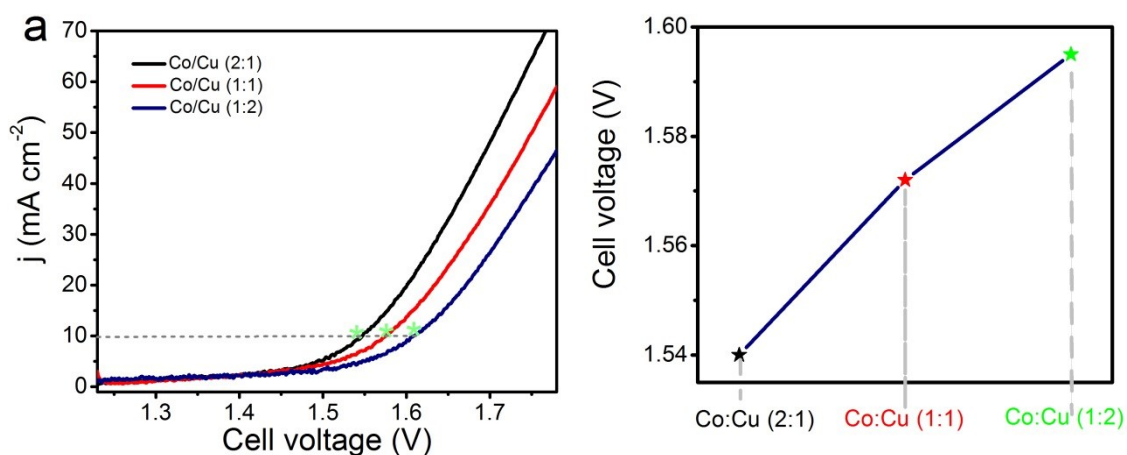
FigureS18.(a) Polarization water splitting curves of CoP@Cu$_2$P-Cu$_3$P with Co: Cu (2:1, 1:1, 2:1) ratio and (b) cell voltage at10 cm^{-2} in 1 m KOH solution at a scan rate of 5 mV s^{-1}.

1-3Supporting Tables:

Table S1. Comparison ofOER activities of mesoporous CoP@Cu$_3$P-Cu$_2$P junction with recently reported electrocatalysts in alkaline electrolyte.

Catalysts	Electrolyte	Mass loading (mg Cm^{-2})	Tafel Slope (mV/dec)	Overpotential at 10 mA cm^{-2} (mV)	Ref
Co/Co$_3$O$_4$@Hollow Carbon	1M KOH	0.40	102.8	391	[4]
CuCo$_2$O$_4$/ NrGO	1M KOH	0.14	64	360	[5]
(Co$_{0.21}$Ni $_{0.25}$Cu$_{0.54}$)$_3$Se$_2$	1M KOH	-	53.3	272	[6]
CuCo$_2$S$_4$	1M KOH	0.70	86.0	310	[7]
CuCo$_2$Se$_4$	1M KOH	0.57	66.5	320	[8]
CuCoP-NC-700	1M KOH	0.20	80	337	[9]
np-(Co$_{0.52}$Fe $_{0.48}$)$_2$P	1M KOH	1.0	30	270	[10]
CoP/ CoCr$_2$O$_4$	1M KOH	0.203	52	290	[11]
CoP/CoP$_2$/Al$_2$O$_3$	1M KOH	0.20	63	300	[12]
CoP/rGO	1M KOH	0.28	66	340	[13]
Co-P/NC	1M KOH	1.0	52	354	[14]
Co$_3$(OH)$_2$(HPO$_4$)$_2$/NF	1M KOH	-	69	240	[15]

CoPc/GO/GC	1M KOH	0.337	61.7	280	[16]
CoP@Cu₃P-Cu₂P	1 M KOH	0.203	72	255	This work

Table S2. Parameters for each catalyst investigated in 1 M KOH.

Catalyst	CoP@Cu$_2$P-Cu$_3$P	CoP	Cu$_3$P	Co$_2$CuO$_4$	IrO$_2$/C
C$_{dl}$ (mF cm^{-2})	6.77	10.05	1.4	1.25	3.5
ESCA (cm^2)	169.25	251	35	31.25	87.5
Intrinsic catalyst activity (mA cm^{-2}) η=370 mV	0.596	0.159	0.21	0.493	0.524

Table S3. Comparison of overall water splitting performance of (-) CoP@Cu$_2$P-Cu$_3$P‖ CoP@Cu$_2$P-Cu$_3$P (+) couple with recently reported Co-based electrocatalysts in alkaline electrolyte.

Catalysts	Substrate	Electrolyte	Mass loading (mg Cm^{-2})	Cell voltage at J$_{10}$ (V)	Stability (h)	Ref
CoP/ CoCr$_2$O$_4$	Ni foam	1M KOH	1.00	1.68	24	[11]
Cr-Doped FeNi–P	Ni foam	1M KOH	3.00	1.50	20	[17]
CoP/CoP$_2$/Al$_2$O$_3$	glassy carbon	1M KOH	0.20	1.65	24	[12]
MoS$_2$/Co$_9$S$_8$/Ni$_3$S$_2$/Ni	Ni foam	1M KOH	-	1.54	24	[18]
CoP-MNA	Ni foam	1M KOH	-	1.62	32	[19]
CoP/rGO	Carbon Paper	1M KOH	0.28	1.70	-	[13]
Co-P/NC	glassy carbon	1M KOH	1.00	1.71	24	[14]
Co$_3$(OH)$_2$(HPO4)$_2$	NF and FFTO-glass	1M KOH	-	1.54	10d	[15]
Ni$_{0.51}$Co$_{0.49}$P	Ni foam	1M KOH	-	1.57	100	[20]
CoP@Cu$_2$P-Cu$_3$P	Ni foam	1M KOH	1.00	1.54	24	This work

1-4 References

[1]Fu, S.; Zhu, C.; Song, J.; Engelhard, M.H.; Li, X.; Du, D.; Lin, Y. Highly Ordered Mesoporous Bimetallic Phosphides as Efficient Oxygen Evolution Electrocatalysts. ACS Energy Letters**2016**, 1(4), 792-796.

[2]Trasatti, S.; Petrii, O.A. Real Surface Area Measurements in Electrochemistry. Pure *Appl. Chem.***1991**, *63*(5), 711-734.

[3] Zhang, Y.; L, Gao.; Hensen, E.J.M.; Hofmann, J.P. Evaluating the Stability of Co2P Electrocatalysts in the Hydrogen Evolution Reaction for Both Acidic and Alkaline Electrolytes. *ACS Energy Lett*. **2018**, 3, 1360−1365.

[4]Bai, C.; Wei, S.; Deng, D.; Lin, X.; Zheng, M.; Dong, Q. A Nitrogen-Doped Nano Carbon Dodecahedron with Co@Co$_3$O$_4$ Implants as a Bi-functional Electrocatalyst for Efficient Overall Water Splitting, *J. Mater. Chem. A*. **2017**, 5(20), 9533-9536.

[5] Bikkarolla, S.K.; Papakonstantinou, P. CuCo$_2$O$_4$ Nanoparticles on Nitrogenated Graphene as Highly Efficient Oxygen Evolution Catalyst. *J. Power Sources***2015**, 281, 243-251.

[6]Cao, X., Johnson, E. and Nath, M., Identifying High-Efficiency Oxygen Evolution Electrocatalysts from Co–Ni–Cu Based Selenides through Combinatorial Electrodeposition. *J. Mater. Chem. A***2019**. 7(16), 9877-9889.

[7]Chauhan, M.; Reddy, K.P.; Gopinath, C.S.; Deka, S. Copper Cobalt Sulfide Nanosheets Realizing a Promising Electrocatalytic Oxygen Evolution Reaction. *ACS Catal* **2017**, 7(9), 5871-5879.

[8]Cao, X.; Medvedeva, J.E.; Nath, M. Copper Cobalt Selenide as a High-Efficiency Bifunctional Electrocatalyst for Overall Water Splitting: Combined Experimental and Theoretical Study. *ACS Applied Energy Materials***2020**. 3(3), 3092-3103.

[9] Zhang, H.; Yang, Z.; Wang, X.; Yan, S.; Zhou, T.; Zhang, C.; Telfer, S.G.; Liu, S. Uniform Copper–Cobalt Phosphides Embedded in N-doped Carbon Frameworks as Efficient Bifunctional Oxygen Electrocatalysts for Rechargeable Zn–air Batteries. *Nanoscale***2019**. 11(37), 17384-17395.

[10]Tan, Y.; Wang, H.; Liu, P.; Shen, Y.; Cheng, C.; Hirata, A.; Fujita, T.; Tang, Z.; Chen, M. Versatile nanoporous bimetallic phosphides towards electrochemical water splitting. *Energy Environ. Sci.***2016**. 9 (7), 2257-2261.

[11]Saad, A.; Shen, H.; Cheng, Z.; Ju, Q.; Guo, H.; Munir, M.; Turak, A.; Wang, J.; Yang, M. Three-Dimensional Mesoporous Phosphide–Spinel Oxide Heterojunctions with Dual Function as Catalysts for Overall Water Splitting. *ACS Appl. Energy Mater***2020**. 3(2) 1684-1693.

[12]Li, W.; Zhang, S.; Fan, Q.; Zhang, F.; Xu, S. Hierarchically Scaffolded CoP/CoP2 Nanoparticles: Controllable Synthesis and their Application as a Well-Matched Bifunctional Electrocatalyst for Overall Water Splitting. Nanoscale. **2017**, 9(17), 5677-5685.

[13] Jiao, L.; Zhou, Y.X.; Jiang, H.L. Metal–Organic Framework-Based CoP/Reduced Graphene Oxide: High-Performance Bifunctional Electrocatalyst for Overall Water Splitting. *Chem. Sci.* **2016**, 7(3), 1690-1695.

[14]You, B.; Jiang, N.; Sheng, M.; Gul, S.; Yano, J.; Sun, Y. High-Performance Overall Water Splitting Electrocatalysts Derived from Cobalt-Based Metal–Organic Frameworks. *Chem. Mater*. **2015,** 27(22), 7636-7642.

[15]Menezes, P.W.; Panda, C.; Walter, C.; Schwarze, M.; Driess, M. A Cobalt-Based Amorphous Bifunctional Electrocatalysts for Water-Splitting Evolved from a Single-Source Lazulite Cobalt Phosphate. *Adv. Funct. Mater*. **2019**, 29, 1808632.

[16]Wu, H.; Chen, Z.; Zhang, J.; Wu, F.; Xiao, F.; Du, S.; He, C.; Wu, Y.; Ren, Z. Generalized Synthesis of Ultrathin Cobalt‐Based Nanosheets from Metallophthalocyanine‐Modulated Self‐Assemblies for Complementary Water Electrolysis. *Small*. **2018**, *14*(5), 1702896.

[17]Wu, Y.; Tao, X.; Qing, Y.; Xu, H.; Yang, F.; Luo, S.; Tian, C.; Liu, M.; Lu, X. Cr‐Doped FeNi‐P Nanoparticles Encapsulated into N‐Doped Carbon Nanotube as a Robust Bifunctional Catalyst for Efficient Overall Water Splitting. Adv. Mater. **2019**. 31(15), .1900178.

[18]Yang, Y.; Yao, H.; Yu, Z.; Islam, S.M.; He, H.; Yuan, M.; Yue, Y.; Xu, K.; Hao, W.; Sun, G.; Li, H. Hierarchical Nanoassembly of MoS$_2$/Co$_9$S$_8$/Ni$_3$S$_2$/Ni as a Highly Efficient Electrocatalyst for Overall Water Splitting in a Wide pH Range, J. Am. Chem. Soc. **2019**, 141, 10417−10430

[19]Zhu, Y.P.; Liu, Y.P.; Ren, T.Z.; Yuan, Z.Y. Self-Supported Cobalt Phosphide Mesoporous Nanorod Arrays: A Flexible

and Bifunctional Electrode for Highly Active Electrocatalytic Water Reduction and Oxidation Adv. Funct. Mater. **2015**, 25, 7337–7347

[20]Yu, J.; Li, Q.; Li, Y.; Xu, C.Y.; Zhen, L.; Dravid, V.P.; Wu, J. Ternary Metal Phosphide with Triple-Layered Structure as a Low-Cost and Efficient Electrocatalyst for Bifunctional Water Splitting Adv. Funct. Mater. **2016**,